THE JOURNAL OF PHYSICAL CHEMISTRY C

Article

pubs.acs.org/JPCC

Photooxidation of 9-Anthraldehyde Catalyzed by Gold Nanoparticles: Solution and Single Nanoparticle Studies Using Fluorescence Lifetime Imaging

Tse-Luen (Erika) Wee,[‡] Luciana C. Schmidt,[‡] and Juan C. Scaiano*

Department of Chemistry and Centre for Catalysis Research and Innovation, University of Ottawa, 10 Marie Curie, Ottawa, Ontario, K1N 6N5, Canada

Supporting Information

ABSTRACT: The photooxidation of 9-anthraldehyde can be catalyzed by colloidal Au nanoparticles (AuNP) or diamond-supported Au nanoparticles (AuNCD) by using LED excitation at 530 nm. Visible irradiation of the plasmon band of AuNP in an acetonitrile solution of 9-anthraldehyde saturated with oxygen or air results in formation of oxidation products, particularly anthraquinone. The reaction does not occur in the dark or without AuNP. It is also inhibited in nitrogen-saturated solution. An enhanced oxidation activity has been observed with AuNCD. We also examined the catalysis by colloidal or supported Au nanoparticles with millisecond real-time resolution using FLIM and TIRFM techniques to observe the time-resolved events leading to the single nanoparticle, single molecule conversion of 9-anthraldehyde into its endoperoxide, eventually to yield anthraquinone.

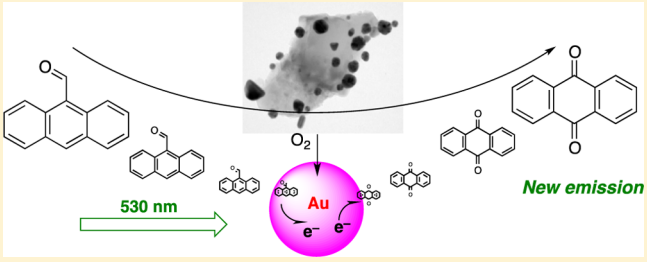

INTRODUCTION

Modern fluorescence microscopy techniques, including Fluorescent Lifetime Imaging Microscopy (FLIM)[1] and Total Internal Reflection Fluorescence Microscopy (TIRFM), are powerful tools in the study of photochemical reactions, and in particular photocatalysis.[2] In this contribution we examine the photooxidation of 9-anthraldehyde initiated by gold surface plasmon band (SPB) excitation, using a combination of solution (ensemble) techniques and single molecule (or single particle) fluorescence techniques to elucidate the mechanism of the conversion of 9-anthraldehyde into its endoperoxide, and its eventual decomposition to yield anthraquinone. Plasmon excitation is a promising methodology to initiate organic photoreactions with fine spatial and temporal control.[3−6]

A few examples of reactions of radical cations and radical anions involving anthracenes have been reported in the literature. For example, the reaction of 9-mesityl-10-methylacridinium ion as an electron transfer (eT) photocatalyst was examined by Kotani et al.,[7] who reported the photocatalytic oxygenation of anthracene and olefins with dioxygen via selective radical coupling. In earlier work, Amatore et al.[8] described the formation of anthraquinone, where the oxidation of anthracene is coupled with the simultaneous reduction of dioxygen in acetonitrile to yield the anthracene radical cation and the superoxide anion.

Nanoparticles, such as metal, metal oxide, and metal sulfide nanoparticles, made of various materials can catalyze many chemical transformations in organic synthesis, including reduction, oxidation, cross coupling, or hydrogenation;[6,9,10] the catalytic properties of gold structures have been reviewed in detail.[10] With advanced transmission microscopy, the structure of individual nanoparticles can be studied down to atomic resolution, but their catalytic properties still have to be measured mainly at the ensemble level.[11,12]

Characterization of catalytic properties is essential to understand the reaction activities, but it is sometimes challenging in ensemble measurements due to the presence of a range of heterogeneous surface sites.[11] The intrinsic heterogeneity, for example, can cause both nanoparticle-dependent and temporally varying catalytic properties. Significant inhomogeneous dynamics and complex local environments can lead to difficult analysis by traditional ensemble-averaged experiments.[12,13] Therefore the single-molecule, single-particle techniques[11,14] can help explore the heterogeneous properties of catalytic reactions, and also compare with the results from standard ensemble (solution) measurements.

Nanocrystalline diamonds (NCD), as a solid carbon-based material, drew attention in various areas in modern technology due to their unique physical properties such as thermal conductivity, hardness, and inertness.[15] They provide an excellent support for catalysts,[16,17] and are also well suited for biotechnological applications.[18] They are biocompatible and chemically inert, and the surface can be easily functionalized with carboxyl and amino groups. Nanosized diamond crystallites, in particular, have a large specific surface area and

Received: September 9, 2012
Revised: October 21, 2012
Published: November 5, 2012

dx.doi.org/10.1021/jp308956y | J. Phys. Chem. C 2012, 116, 24373−24379

after treatment in strong oxidation acid, they show an exceptionally high affinity for proteins in aqueous solution, and this property also can be applied to metal nanoparticle association.[15,19] Gold on diamond nanoparticles prepared as a highly efficient Fenton catalyst reactivity has been reported recently. The gold derived from $HAuCl_4$ has been supported by the conventional deposition/precipitation method on Fenton-treated diamond nanoparticles followed by hydrogen reduction at 300 °C.[17]

In this report we examine the catalytic reactions of 9-anthraldehyde with colloidal or diamond-supported Au nanoparticles. We further tested the electron transfer (eT) driven catalysis of colloidal or supported Au nanoparticles with single-particle detection techniques in millisecond real-time resolution, which is capable of probing complex systems and revealing the dynamics of surface plasmon mediated reactions involving gold.

EXPERIMENTAL SECTION

Material and Methods. The reagents 9-anthraldehyde and gold(III) tetrachloroauric acid hydrate ($HAuCl_4 \cdot 3H_2O$) were commercial products from Sigma and were used as received. 2-Hydroxy-1-[4-(2-hydroxyethoxy)phenyl]-2-methyl-1-propanone (I-2959) was from Ciba Specialty Chemicals; I-2959 was recrystallized from ethyl acetate prior to use. Doubly distilled deionized water was obtained from a Milli-Q system (18 MΩ resistance), while spectroscopic grade acetonitrile purchased from Fisher Scientific was used after drying.

We have reported on the facile photochemical synthesis for different types of metal nanoparticles.[4,20,21] The colloidal Au nanoparticles were made by reduction of $HAuCl_4$ in deionized water by using Irgacure I-2959 as photoreducing agent, followed by UVA irradiation for 15 min at room temperature (Scheme 1).[20]

Scheme 1. Mechanism for the Formation of AuNP through Ketyl Radical Reduction of Au(III)

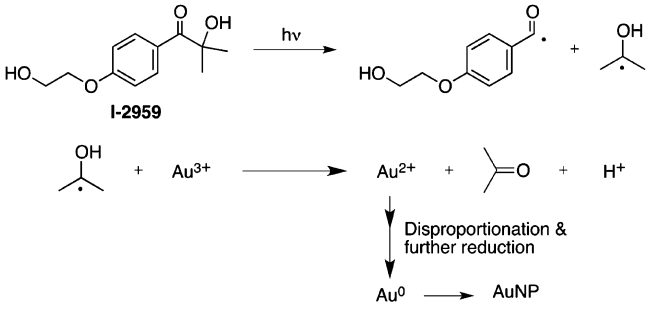

Nanocrystalline diamond supported gold (AuNCD) was made with the same method as colloidal gold. The commercially available synthetic nanodiamonds were purchased from Elementsix (Micron+MDA), with an average diameter of 150 nm. A solution containing a mixture of 3.3×10^{-4} M $HAuCl_4$, 10×10^{-4} M I-2959, and 5 mg/mL of 150 nm diamond suspension in doubly distilled deionized water (milli-Q system, 18 MΩ resistance) was employed as a AuNCD precursor. Samples were irradiated with use of a 24 Cell Culture well plate (Corning, USA), placed in a Luzchem LZC-4 V photoreactor equipped with up to 14 UVA lamps for 15 min.

Upon UVA irradiation, the light yellow milky solution of $HAuCl_4$ with diamonds gradually turned reddish, and the positive metal ions were first randomly adsorbed onto the imperfections sited on the diamond surface due to the electrostatic attraction, followed by coordinated nucleation on the diamond imperfection sites starts.[17] The excess of gold colloids and I-2959 was removed performing centrifugation-redispersion with Milli-Q water.

A starting volume of 8 mL was centrifuged at 4500 rpm for 1 h, and the supernatant removed. The remaining AuNCD were immediately resuspended in 0.8 mL of H_2O. The sample solution for the plasmon-mediated catalysis was prepared by adding 200 μL of diamond-supported AuNP to 1 mL of 1 mM 9-anthraldehyde.

The reaction between 9-anthraldehyde (1 mM) and colloidal Au nanoparticles (AuNP) or diamond-supported AuNP (AuNCD) (4 nM) was performed in acetonitrile under air or oxygen, using a 530 nm LED system, for 3 h. The LED system is equipped with four, 530 nm LedEngin 10 W LZ4−40G110 emitters attached to aluminum heat sinks in a custom-design irradiator, using a fan to minimize temperature effects. After excitation, the irradiated samples were extracted with ethyl acetate/water mixture and characterized by gas chromatography−mass spectrometry (GC-MS). We note that under these conditions any endoperoxides are converted predominantly to anthraquinone (vide infra). For NMR analysis of the intermediates the reaction was performed in acetone-d_6 and the crude sample was analyzed.

To detect the presence of endoperoxides, the reaction was run in acetone-d_6. After 2 h of irradiation with LEDs the corresponding endoperoxide was detected by using NMR techniques and shows the signature signals[22] of the H-atoms in the 9,10 positions (see SI, Figure S3).

TEM Characterization. The morphologies and microstructures of colloidal AuNP or supported gold on diamond were recorded by TEM, using a field-emission transmission spectrum microscope (JEOL JEM-2100F) equipped with an ultrahigh-resolution pole piece operating at 200 kV. Approximately 10 μL of solution was delivered to a carbon-coated copper grid (400 mesh, EMS), and turbo-pumped in a vacuum system prior to imaging. The average particle diameter of colloidal Au nanoparticles on diamond was 8 nm. From the TEM images, the nucleation of gold nanocrystals on the diamond surface can be clearly seen; the average size of the AuNP on the diamond surface is about 22 nm. The total Au content of the final Au-diamond catalyst was about 3% by weight.

Single-Particle Fluorescence Spectroscopy and Imaging. *Sample Preparation.* Coverslips (Fisher) were thoroughly cleaned by H_2SO_4 and H_2O_2, and then dried to render their surfaces hydrophilic. The glass substrates were sandwiched with 20 μL of ethanol solution of 5% 3-aminopropyltrimethoxysilane, rinsed with ethanol, and blow-dried with N_2. The resulting glass substrates, modified with the silane-coupling agent, were sandwiched with 20 μL of 1 nM colloidal solution of AuNCD for an hour, then dried. These colloidal or supported Au nanoparticles were prepared from photosynthetic methods as described above.

The oxidation of 9-anthraldehyde was also examined with a Fluorescent Lifetime Imaging System (FLIM, PicoQuant). The instrument is equipped with a frequency doubled picosecond pulse diode laser (530.6 nm, 100 ps, 40 MHz, LDH-P-FA-530L, PicoQuant). The laser beam was collimated and focused through a fiber-coupling unit. A beam splitter Z532rdc (Chroma) was used to reflect the excitation light into the oil

dx.doi.org/10.1021/jp308956y | J. Phys. Chem. C 2012, 116, 24373−24379

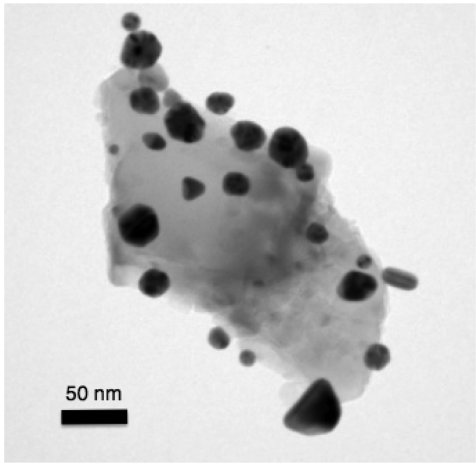

Figure 1. TEM image of AuNP on the NCD support; the smaller, darker spots due to AuNP can be seen on the diamond support.

immersion TIR (total internal reflection) objective (100×, NA1.45, Olympus, PLAPO). The excitation dose (average power) is about 0.5 μW for all samples. The 530 nm laser wavelength was chosen because it is best suited for the SPB of spherical AuNP. The system is similar to that described in the literature,[13] except for the addition of FLIM capabilities.

We studied the single-molecule eT dynamics of 9-anthraldehyde and AuNCD by probing the single-particle intensity time trajectories and images. Single-particle fluorescence images and fluorescence intensity trajectories were recorded and processed through single-photon-counting module (τ-SPAD-100, PicoQuant), Time Correlated Single Photon Counting Module (TSCPC), and SymPhoTime program (PicoQuant).

RESULTS

Solution Photooxidation of 9-Anthraldehyde with Gold Nanoparticle Catalysis. A number of experiments were performed, both with colloidal AuNP and with diamond-supported gold (AuNCD), in order to establish the role and importance of the various parameters involved. As shown in Table 1, entry 4, exposure of 9-anthraldehyde in the presence of colloidal AuNP for 3 h with 530 nm LED excitation resulted in 23% conversion to anthraquinone. Under the same excitation conditions but with AuNCD, Table 1, entry 5, the best conversion efficiency of 81% to anthraquinone is achieved, which is about 3.5 times higher than that with AuNP. The oxidation reaction does not occur without the AuNP (Table 1, entry 1) or in the dark (Table 1, entries 2 and 3). It also can be inhibited when oxygen is removed (Table 1, entry 11). Clearly oxygen plays a crucial role in the oxidation. However, the reaction efficiency is not enhanced in an oxygen atmosphere compared with an air atmosphere (Table 1, entry 6). The equilibrium concentration of oxygen in acetonitrile under 1 atm of oxygen is 8.00 mM and approximately one-fifth of this value under 1 atm of air,[23] which is still sufficient to react with 1 mM 9-anthraldehyde.

Table 1. Oxidation of 9-Anthraldehyde[a]

entry	excitation	conditions[a]	catalyst[b]	yield,[c] %
1	530 nm LED	air	–	0
2	dark	air	AuNP	0
3	dark	air	AuNCD	0
4	530 nm LED	air	AuNP	23
5	530 nm LED	air	AuNCD	81
6	530 nm LED	O_2	AuNCD	82
7	530 nm LED	air/*N*,*N*-dimethylaniline[d]	AuNCD	0
8	530 nm LED	air/*N*,*N*-dimethylaniline	AuNP	0
9	530 nm LED	air/*p*-dinitrobenzene	AuNCD	80
10	530 nm LED	air/*p*-dinitrobenzene	AuNP	25
11	530 nm LED	N_2	AuNCD	0

[a]Reaction performed with 9-anthraldehyde (1 mM) in acetonitrile as a solvent for 3 h. [b]AuNP or AuNCD 4 nM. [c]Quantification of anthraquinone by gas chromatography using standard internal methods. Error <5%. [d]Together with 8% *N*-methylaniline.

We propose below a mechanism that involves electron transfer from 9-anthraldehyde to plasmon-excited gold nanoparticles. To test the proposed mechanism, two sets of experiments were performed with use of competitive electron donors and acceptors (entries 7, 8, 9, and 10 in Table 1).

When the reaction is performed with AuNCD in the presence of *N*,*N*-dimethylaniline which is a better electron donor than 9-anthraldehyde, the yield of anthraquinone is 0%, and a small amount of *N*-methylaniline is detected (see SI, Figure S2). This experiment suggests that *N*,*N*-dimethylaniline can substitute for 9-anthraldehyde as the electron donor, and in the process suppress the oxidation of 9-anthraldehyde. Further, when *p*-dinitrobenzene, a good electron acceptor, is added, the reaction in not inhibited (Table 1, entries 9 and 10). These results are consistent with the electron transfer mechanism proposed below.

The endoperoxide derived from 9-anthraldehyde was characterized in experiments run in acetone-d_6 and using NMR as the analytical technique (see SI, Figure S3). This result is in accordance with previous work by Kotani et al.[7] and Amatore et al.[8] where the oxidation of anthracene is coupled with the simultaneous reduction of dioxygen in acetonitrile to yield the anthracene radical cation and the superoxide anion, with the final production of anthraquinone. Figure 2 shows the mechanism proposed and on which we elaborate in the Discussion section.

Single-Molecule, Single-Particle Fluorescence Imaging. Fluorescence lifetime data measured by using confocal microscopy with a time-correlated single-photon counting system (TCSPC) allowed us to study the catalytic photooxidation of 9-anthraldehyde molecules eventually leading to anthraquinone through the excitation of the surface plasmon band of AuNP at ~530 nm.

Figure 3 shows the fluorescence lifetime images for single Au particles interact with 9-anthraldehyde on a clean cover glass during 530 nm excitation. The fluorescence trajectories (Figure 4) show significant fluctuation and blinking at subsecond to second time scales. The fluorescence burst from the product can be easily distinguished from the background signal of 9-anthraldehyde in solution. In some trajectories, many fluorescence bursts show multiple on-levels, indicating a new molecule of anthraquinone formed on the AuNP surface before an earlier product diffused away, dissociated from the AuNP or otherwise photobleaches.

To further understand the mechanism for the formation of anthraquinone, we have measured the fluorescence decay kinetics under different experimental conditions with our TCSPC system, part of the FLIM instrument. The time gated fluorescence distribution along the *y*-axes from the time traces gave us single-molecule fluorescence decay curves. Figure

dx.doi.org/10.1021/jp308956y | J. Phys. Chem. C 2012, 116, 24373−24379

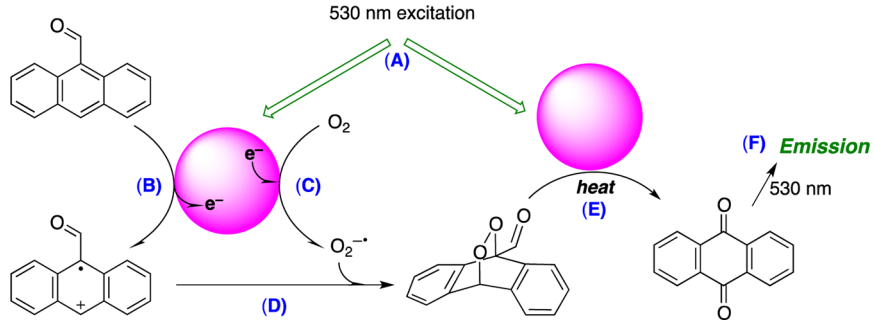

Figure 2. Proposed reaction mechanism. The colored circles represent the AuNP (supported or not) and the blue letters in parentheses the various steps in the reaction.

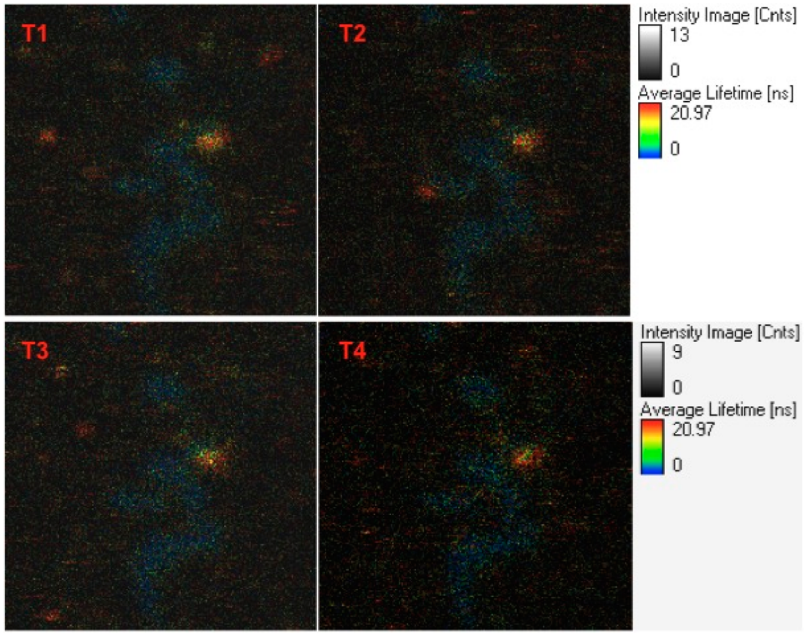

Figure 3. Fluorescence lifetime image (6.6 μm × 6.6 μm, 200 × 200 pixels) of single AuNP catalysis. Fluorescent spots with longer lifetime (red dots), from T1 to T4, are due to the fluorescent product after surface plasmon excitation (530 nm) of AuNP.

5 shows the fluorescence decay observed during the 530 nm excitation, with and without AuNP in solution. The fluorescence decay profiles were fitted by the biexponential function. From the decay curve, it can be clearly seen that the second decay component showed up after the reaction with gold, from the formation of anthraquinone during 530 nm excitation. In the absence of gold the lifetime was 2.08 ns, while the approximately biexponential decay after reaction had components with 6.4 and 0.94 ns. A different approach is shown below in Figure 6.

The fluorescence lifetime histogram (Figure 6) and fluorescence intensity and lifetime correlograms show that, without interaction with AuNCD, the fluorescence lifetime distribution is in a range of 1 to 3 ns, and the fluorescence lifetime histogram after interaction with gold nanoparticles shows broad fluorescence lifetime fluctuation in a range of 4 to 8 ns with a minor short component. The results are consistent with the simple analysis of Figure 5.

We also used the TIRF microscope system to investigate the photocatalytic oxidation of 9-anthraldehyde on individual Au nanoparticles (see Movie S8, Supporting Information). The TIRFM movie shows several individual blinking sites on Au nanoparticle in DMSO solution containing 1 mM 9-anthraldehyde under 543 nm irradiation. A number of fluorescence bursts with signals much higher than the background were observed during photoirradiation.

Control experiments confirmed that AuNP, 9-anthraldehyde, and 532 nm excitation are all-essential to the generation of fluorescence bursts. No digital fluorescence burst was observed in the absence of AuNP, or 9-anthraldehyde. The average τ_{on} is much shorter than the photobleaching lifetime of 9-anthraldehyde under the same laser intensity, thus the intensity decrease of the fluorescence trajectory is not due to 9-anthraldehyde photobleaching. All the results were reproducible by using DMSO, acetonitrile, or acetonitrile/water mixture as solvent.

■ DISCUSSION

Our results show that colloidal AuNP or supported AuNCD can be successfully employed in the plasmon-mediated radical-cation oxidation of 9-anthraldehyde, with the latter showing improved yields. Both fluorescence data and chromatographic analysis show that formation of anthraquinone can be achieved photochemically through 530 nm LED excitation. We note that the decomposition of endoperoxides, thermally or photochemically, can yield a variety of products,[24] including "photo-

dx.doi.org/10.1021/jp308956y | J. Phys. Chem. C 2012, 116, 24373−24379

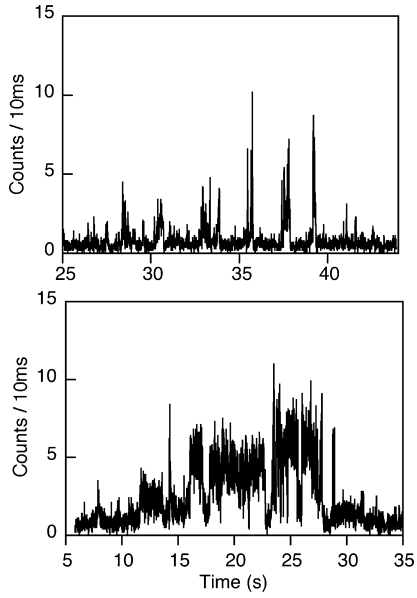

Figure 4. A segment of the fluorescence trajectory from the fluorescence spots of FLIM images. Top: Fluorescence bursts from the reaction of 9-anthraldehyde with AuNP (events) on the AuNP surface during the reaction. Bottom: Fluorescence bursts from the reaction of 9-anthraldehyde with AuNCD.

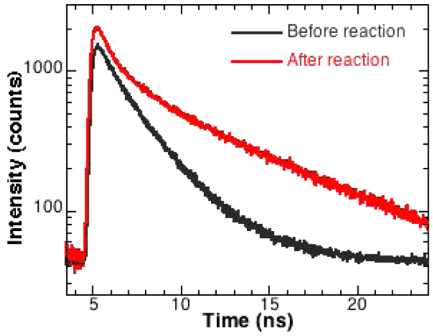

Figure 5. Fluorescence decay profile before and after the oxidation of 9-anthraldehyde with AuNCD as photocatalyst.

reversion" (yielding singlet oxygen), and the quinone pathway observed here. The decomposition to give predominantly the quinone is not unprecedented in cases where the decomposition occurs on a surface.[25]

Studies in solution show unequivocally that the gold catalyst, light, and oxygen are all essential for the oxidation of 9-anthraldehyde to occur. Further, the fact that usage of oxygen or air has no effect on the oxidation efficiency suggests that step B, rather than C, is rate controlling (see Figure 2).

One may wonder if the last steps in the reaction, specifically step E in Figure 2, actually require AuNP or light. For this purpose the TIRFM data of Figure 7 are critical. First let us note that samples prepared for the purpose of endoperoxide studies (see the SI) survive long enough to allow for extensive handling and analysis. It is thus highly unlikely that the conversion to anthraquinone occurs spontaneously at room temperature, as it would also be counter to the vast knowledge on the stability of endoperoxides.[24] Further, TIRFM only sees molecules within the very narrow evanescent field, and molecules not associated with a given particle are not detectable. Thus, surface spots showing blinking, as in Figure

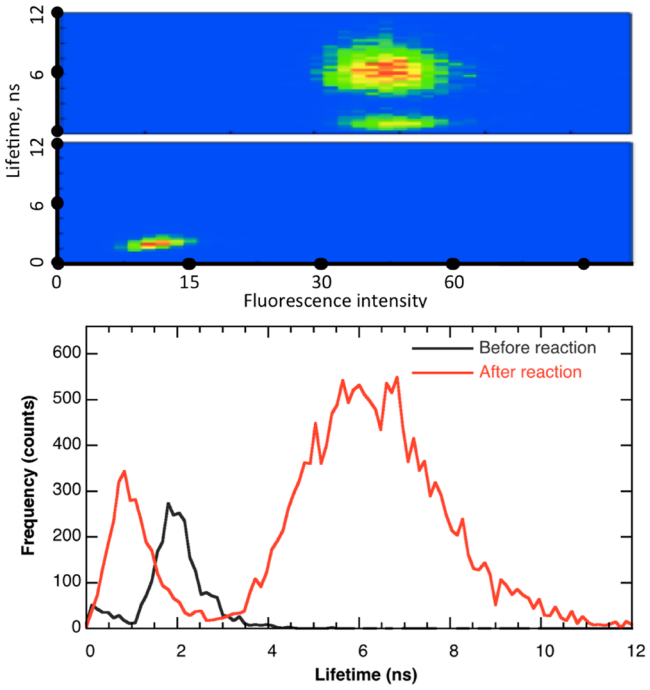

Figure 6. Fluorescence lifetime histogram (bottom) and correlogram before (middle) and after (top) the photoreaction of 9-anthraldehyde catalyzed by AuNCD.

7, are indicative of fluorescence-inducing chemical changes occurring at anchored particles as a result of plasmon excitation, i.e., step E in Figure 2. In other words endoperoxide decomposition to yield quinones is favored at surfaces, as expected.[25] Consistently with this, the same surface spots "blink", that is emit and go dark as the catalytic process proceeds. FLIM laser excitation fulfills two roles after the endoperoxide has been formed. First it must generate enough heat to cause endoperoxide decomposition, a process that can reach 500 °C for submicrosecond times at the AuNP surface.[26] Second, the product must be excited for it to show fluorescence (step F in Figure 2), a process that could be the subject of enhanced plasmon absorption/emission (vide infra).[27,28]

The results show that in each trajectory to a single AuNP, each fluorescence burst comes from one of the many possible active sites on the surface of the nanoparticle; the results also demonstrate the surface plasmon band mediated activity intermittency reflected by single-molecule fluorescence fluctuations. The results do not show if an endoperoxide molecule decomposes immediately upon arrival at a surface site, or if there is a delay until reaction occurs. Most likely molecules wait until a suitable thermal change[5,26] is triggered by plasmon excitation.

We were surprised at the ease with which single molecule anthraquinone emissions were acquired, given that the excitation laser and bandpass filter in use force emissions to be recorded only at $\lambda > 550$ nm, i.e., the red edge of the anthraquinone emission. It is likely that plasmon-induced fluorescence enhancements provide unexpected help with these measurements.[27,29]

CONCLUSION

Gold nanoparticles promote the oxidation reaction of 9-anthraldehyde in acetonitrile, under irradiation of the gold plasmon band, in the presence of air or oxygen. Enhanced

dx.doi.org/10.1021/jp308956y | J. Phys. Chem. C 2012, 116, 24373−24379

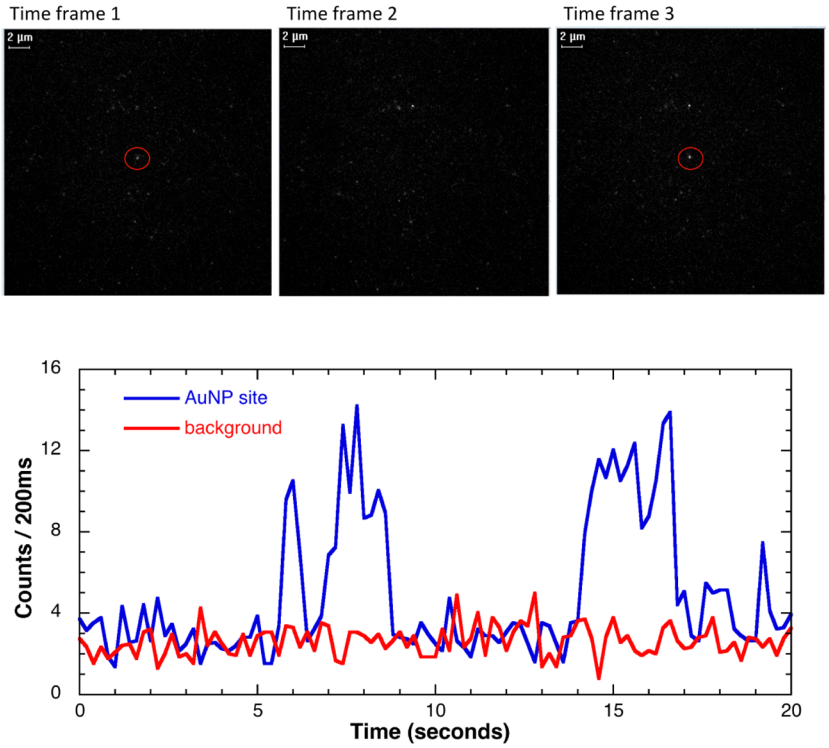

Figure 7. Still images (top) extracted from the TIRF movie available in the SI showing the point in the image selected for the trajectory shown at the bottom. Note that the point selected is bright in time frames 1 and 3, but dark in time frame 2, showing that this AuNP blinks as the reaction occurs.

conversion efficiency was observed with AuNCD. No conversion was observed in the absence of AuNP, AuNCD, or 9-anthraldehyde or in the absence of O_2. The on and off fluorescence burst traces and the TIRFM images show multiple catalytic events located at the same particle spot (same or vicinal docking site). Fluorescence lifetime changes were observed under the excitation of the surface plasmon band at 530 nm of AuNP or AuNCD with 9-anthraldehyde. No fluorescence burst trajectory was observed in the absence of either AuNP or AuNCD or 9-anthraldehyde. Simple diffusion of free 9-anthraldehyde in the solution could not be the cause of the digital trajectories observed.

■ ASSOCIATED CONTENT

Ⓢ Supporting Information

Details on chromatographic analysis, NMR data, fluorescence trajectory histogram data, and fluorescence spectra and a TIRF movie. This material is available free of charge via the Internet at http://pubs.acs.org.

■ AUTHOR INFORMATION

Corresponding Author

*E-mail: tito@photo.chem.uottawa.ca.

Author Contributions

‡Equal contribution.

Notes

The authors declare no competing financial interest.

■ ACKNOWLEDGMENTS

We thank the Canadian Foundation for Innovation and the Natural Sciences and Engineering Research Council (Canada) for generous financial support under its Discovery, CRD, CREATE, and scholarships programs. The assistance of Mr. Michel Grenier with LED experiments is gratefully acknowledged.

■ REFERENCES

(1) Gadella, T. W. J., Jr.; Jovin, T. M.; Clegg, R. M. *Biophys. Chem.* **1993**, *48*, 221−239. Heuff, R. F.; Swift, J. L.; Cramb, D. T. *Phys. Chem. Chem. Phys.* **2007**, *9*, 1870−1880.

(2) Roeffaers, M. B. J.; Hofkens, J.; De Cremer, G.; De Schryver, F. C.; Jacobs, P. A.; De Vos, D. E.; Sels, B. F. *Catal. Today* **2007**, *126*, 44−53.

(3) Nabika, H.; Takase, M.; Nagasawa, F.; Murakoshi, K. *J. Phys. Chem. Lett.* **2010**, *1*, 2470−2487. Stamplecoskie, K. G.; Fasciani, C.; Scaiano, J. C. *Langmuir* **2012**, *28*, 10957−10961.

(4) Scaiano, J. C.; Netto-Ferreira, J. C.; Alarcon, E.; Billone, P.; Alejo, C. J. B.; Crites, C. O. L.; Decan, M.; Fasciani, C.; Gonzalez-Bejar, M.; Hallett-Tapley, G.; et al. *Pure Appl. Chem.* **2011**, *83*, 913−930.

(5) Bakhtiari, A. B. S.; Hsiao, D.; Jin, G.; Gates, B. D.; Branda, N. R. *Angew. Chem., Int. Ed.* **2009**, *48*, 4166−4169.

(6) Christopher, P.; Xin, H.; Linic, S. *Nat. Chem.* **2011**, *3*, 467−472.

(7) Kotani, H.; Ohkubo, K.; Fukuzumi, S. *J. Am. Chem. Soc.* **2004**, *126*, 15999−16006.

(8) Amatore, C.; Brown, A. R. *J. Am. Chem. Soc.* **1996**, *118*, 1482−1486.

(9) Oregan, B.; Gratzel, M. *Nature* **1991**, *353*, 737−740.

(10) Corma, A.; Garcia, H. *Chem. Soc. Rev.* **2008**, *37*, 2096−2126.

(11) Xu, W.; Kong, J. S.; Yeh, Y.-T. E.; Chen, P. *Nat. Mater.* **2008**, *7*, 992−996.

(12) Wang, Y. M.; Wang, X. F.; Ghosh, S. K.; Lu, H. P. *J. Am .Chem. Soc.* **2009**, *131*, 1479−1487.

(13) Tachikawa, T.; Majima, T. *Langmuir* **2009**, *25*, 7791−7802.

(14) DeCremer, G.; Roeffaers, M. B. J.; Bartholomeeusen, E.; Lin, K.; Dedecker, P.; Pescarmona, P. P.; Jacobs, P. A.; DeVos, D. E.; Hofkens, J.; Sels, B. F. *Angew. Chem., Int. Ed.* **2010**, *49*, 908−911. Tachikawa, T.; Majima, T. *Langmuir* **2012**, *28*, 8933−8943.

(15) Krueger, A.; Stegk, J.; Liang, Y. J.; Lu, L.; Jarre, G. *Langmuir* **2008**, *24*, 4200−4204.

(16) Shi, X. Q.; Jiang, X. H.; Lu, L. D.; Yang, X. J.; Wang, X. *Mater. Lett.* **2008**, *62*, 1238−1241.
(17) Navalon, S.; Martin, R.; Alvaro, M.; Garcia, H. *Angew. Chem., Int. Ed.* **2010**, *49*, 8403−8407.
(18) Liu, K. K.; Zheng, W. W.; Wang, C. C.; Chiu, Y. C.; Cheng, C. L.; Lo, Y. S.; Chen, C. P.; Chao, J. I. *Nanotechnology* **2010**, *21*, ?. Wee, T. L.; Mau, Y. W.; Fang, C. Y.; Hsu, H. L.; Han, C. C.; Chang, H. C. *Diamond Relat. Mater.* **2009**, *18*, 567−573.
(19) Liu, Y.; Gu, Z. N.; Margrave, J. L.; Khabashesku, V. N. *Chem. Mater.* **2004**, *16*, 3924−3930.
(20) McGilvray, K. L.; Decan, M. R.; Wang, D.; Scaiano, J. C. *J. Am. Chem. Soc.* **2006**, *128*, 15980−15981.
(21) McGilvray, K. L.; Scaiano, J. C. In *CRC Handbook of Organic Photochemistry and Photobiology*, 3rd ed.; Griesbeck, A., Oelgemoeller, M., Ghetti, F., Eds.; CRC Press: Boca Raton, FL, 2012.
(22) Carney, J. M.; Hammer, R. J.; Hulce, M.; Lomas, C. M.; Miyashiro, D. *Tet. Letters* **2011**, *52*, 352−355.
(23) Turro, N. J.; Ramamurthy, V.; Scaiano, J. C. *Modern Molecular Photochemistry of Organic Molecules*; University Science Publishers: New York, NY, 2010.
(24) Aubry, J.-M.; Pierlot, C.; Rigaudy, J.; Schmidt, R. *Acc. Chem. Res.* **2003**, *36*, 668−675.
(25) Debestani, R.; Ellis, K. J.; Sigman, M. E. *J. Photochem. Photobiol. A: Chem.* **1995**, *86*, 231−239.
(26) Fasciani, C.; Bueno Alejo, C. J.; Grenier, M.; Netto-Ferreira, J. C.; Scaiano, J. C. *Org. Lett.* **2011**, *13*, 204−207.
(27) Anger, P.; Bharadwaj, P.; Novotny, L. *Phys. Rev. Lett.* **2006**, *96*, 113002.
(28) Pacioni, N. L.; González-Bejar, M.; Alarcón, E.; McGilvray, K. L.; Scaiano, J. C. *J. Am .Chem. Soc.* **2010**, *132*, 6298−6299.
(29) Bharadwaj, P.; Novotny, L. *Opt. Express* **2007**, *15*, 14266−14274.